NIH Public Access
Author Manuscript
Nanotoxicology. Author manuscript; available in PMC 2010 September 7.

Published in final edited form as:
Nanotoxicology. 2008 March ; 2(1): 33–42. doi:10.1080/17435390701882478.

Does Nanoparticle Activity Depend upon Size and Crystal Phase?

Jingkun Jiang[1], **Günter Oberdörster**[2], **Alison Elder**[2], **Robert Gelein**[2], **Pamela Mercer**[2], and **Pratim Biswas**[1]

Günter Oberdörster: gunter_oberdorster@urmc.rochester.edu; Pratim Biswas: pratim.biswas@wustl.edu

[1] Aerosol and Air Quality Research Laboratory, Department of Energy, Environmental & Chemical Engineering, Washington University in St. Louis, St. Louis, USA, Phone: +001-314-935-5464

[2] Department of Environmental Medicine, University of Rochester, Rochester, USA, Phone: +001-585-275-3804

Abstract

A method to investigate the dependence of the physicochemical properties of nanoparticles (e.g. size, surface area and crystal phase) on their oxidant generating capacity is proposed and demonstrated for TiO_2 nanoparticles. Gas phase synthesis methods that allow for strict control of size and crystal phase were used to prepare TiO_2 nanoparticles. The reactive oxygen species (ROS) generating capacity of these particles was then measured. The size dependent ROS activity was established using TiO_2 nanoparticles of 9 different sizes (4 – 195 nm) but the same crystal phase. For a fixed total surface area, an S-shaped curve for ROS generation per unit surface area was observed as a function of particle size. The highest ROS activity per unit area was observed for 30 nm particles, and observed to be constant above 30 nm. There was a decrease in activity per unit area as size decreased from 30 nm to 10 nm; and again constant for particles smaller than 10 nm. The correlation between crystal phase and oxidant capacity was established using TiO_2 nanoparticles of 11 different crystal phase combinations but similar size. The ability of different crystal phases of TiO_2 nanoparticles to generate ROS was highest for amorphous, followed by anatase, and then anatase/rutile mixtures, and lowest for rutile samples. Based on evaluation of the entire dataset, important dose metrics for ROS generation are established. Their implications of these ROS studies on biological and toxicological studies using nanomaterials are discussed.

1. Introduction

Advances in nanotechnology have been touted to be very promising with applications in a large number of disciplines, and projected to be a trillion dollar market by 2015 (Maynard 2007; Roco 2004). A key factor is that the building blocks, nanoparticles, have unique physicochemical properties and functionalities that are different from their bulk counterparts (Harman et al. 2002; McDonald et al. 2005). In recent years, there has been an increased concern about the potential of these nanoparticles to be emitted to the environment, followed by exposure of human beings and resultant adverse health effects (Biswas and Wu 2005; Oberdorster 2004; Wiesner et al. 2006). There is supporting evidence of adverse health effects following exposure to nanoparticles present in the atmosphere and from combustion source emissions (Donaldson et al. 2002; Donaldson et al. 2001; Donaldson and Tran 2002; Penttinen et al. 2001; Wichmann and Peters 2000). Due to the importance of this size class of particles, the term nanotoxicology has been coined that aims to establish the relationship between

Corresponding Author: Pratim Biswas, PhD, Professor, Department of Energy, Environmental & Chemical Engineering, Campus Box 1180, Washington University in St. Louis, St. Louis, MO 63130, USA, Telephone: 314-935-5482, Fax: 314-935-5464, pratim.biswas@wustl.edu.

NIH-PA Author Manuscript
NIH-PA Author Manuscript
NIH-PA Author Manuscript

NIH-PA Author Manuscript

NIH-PA Author Manuscript

NIH-PA Author Manuscript

nanoparticle physicochemical properties (e.g. size, surface properties and crystal phase) and their toxic potential (Oberdorster et al. 2005a; Oberdorster et al. 2005b; Oberdorster et al. 2007).

In spite of the large number of studies aimed at establishing the biological activity of nanoparticles and the influence of important physico-chemical parameters such as size, surface properties, crystal phase and others (Hoshino et al. 2004; Magrez et al. 2006; Oberdorster et al. 2005b); the use of appropriate dose metrics needs to be carefully considered. For example, to determine the effect of size of the nanoparticle on biological activity, should comparisons of activity or biological response be based on the mass of the sample, as is done in conventional toxicological studies, or should the metric be total surface area when comparing effects of different sized particles?

There is still uncertainty in the current understanding of the relationship between physico-chemical parameters and potential toxicological effects. For example, there have been several recent studies on the toxicity evaluation of nanosized titanium dioxide (a widely used nanomaterial) and establishing a relationship to physico-chemical characteristics (Oberdorster 2000; Oberdorster et al. 2005b; Sayes et al. 2006; Warheit et al. 2007; Warheit et al. 2006). Warheit and co-workers recently dosed the lungs of rats with 3 sizes of titanium dioxide nanoparticles and suggested that toxicity is not dependent upon particle size or surface area (Warheit et al. 2006). A clear conclusion regarding particle size could not be reached as only 3 sizes were tested, of which one was of a different crystal phase, and the two of the same crystal phase (rutile) were of different shapes (rods, ~200 nm × 40 nm, and dots, ~10 - 20 nm). In a follow up study, these authors tested the pulmonary toxicity of 3 sizes (hydrodynamic diameter: 136 nm, 149 nm and 382 nm) of the rutile phase with alumina surface coating, and compared it to 25 nm TiO_2 particles (of a different crystal phase) (Warheit et al. 2007). In a third study, they examined the toxic potential of 3 samples of different crystal phases, however, the sizes were also different (Sayes et al. 2006). Surface properties were proposed to account for the differences in biological responses. Oberdörster et al (Oberdorster 2000; Oberdorster et al. 2005b) conducted pulmonary toxicity tests with 20 nm (80% anatase) and 250 nm (100% anatase) titanium dioxide particles and found that the total surface area was a metric that related to neutrophil lung inflammation in rats. No clear trends with regard to the influence of TiO_2 crystallinity and particle size on biological activity could be seen in these different studies and contrasting concepts were proposed. One major reason was the paucity of different well-characterized TiO_2 samples (in terms of size and crystallinity) that were used, thus precluding the development of convincing conclusions about the function of parameters such as particle size or crystal phase.

Recent developments in aerosol route synthesis of these materials allow for greater and independent control of physico-chemical properties such as size, shape and crystal phase (Jiang et al. 2007). Flame aerosol reactors have been used in several studies (Thimsen and Biswas 2007; Wegner and Pratsinis 2003; Yang et al. 1996), and are also a preferred route of production of nanomaterials in industrial scale systems (Rosner 2005). Recent studies have illustrated the potential of varying these parameters in a well controlled manner and have demonstrated the synthesis of titanium dioxide nanoparticles over a range of sizes.

While toxicological effects are usually evaluated by *in vitro* and *in vivo* studies, a rapid cell-free pre-screening assay to determine the intrinsic potential of particles to generate reactive oxygen species (ROS) could be informative as well (Venkatachari et al. 2005). Both *in vitro* and *in vivo* tests of engineered nanoparticles (e.g. carbon nanotubes, TiO_2 and quantum dots) indicate that ROS production is related to their toxicity (Donaldson et al. 2006; Hoshino et al. 2004; Oberdorster et al. 2007). In this study, the oxidant generating potential in a cell-free

NIH-PA Author Manuscript

NIH-PA Author Manuscript

NIH-PA Author Manuscript

medium has been used as a pre-screening method to evaluate the dependence of the TiO_2 reactivity on physico-chemical properties.

The objective of the study is to evaluate an appropriate dose metric for oxidant generation to establish the role of particle size and crystal phase of a model nanoparticle, titanium dioxide. The hypothesis is that both size and crystallinity will impact oxidant generation. The primary limitation of few samples in previous studies reported in the literature has been overcome by synthesizing a large number of well defined samples (i) over a range of sizes with the same crystal phase, and (ii) of different crystal phases with the same size using flame aerosol reactors (FLAR). Finally, the relevance and guidelines for analyzing the data from toxicological studies are also presented.

2. Method

2.1 Nanoparticle Synthesis and Characterization

Nanosized TiO_2 samples were prepared using several gas phase synthesis methods: a diffusion flame aerosol reactor (Jiang et al. 2007), a premixed flame aerosol reactor (Thimsen and Biswas 2007), a furnace aerosol reactor (Namiki et al. 2005; Okuyama et al. 1986), and a spark aerosol reactor (Kreyling et al. 2002). The diffusion flame aerosol reactor was used to synthesize TiO_2 nanoparticles with large size ($\geq$ 30 nm) and different crystal structures (anatase; anatase and rutile mixtures). Anatase TiO_2 nanoparticles with small sizes ($\leq$ 20 nm) were made in the premixed flame aerosol reactor. The furnace aerosol reactor was utilized to make amorphous TiO_2 particles with large sizes. The precursor used to synthesize TiO_2 particles was titanium tetra-isopropoxide (TTIP, 97%, Aldrich), and was fed into the reactors either by an atomizer or a bubbler. The properties of TiO_2 nanoparticles were controlled by adjusting the reactant feed rates and the temperature-time history in these reactors. Amorphous TiO_2 nanoparticles with small sizes were produced using a spark aerosol generator as reported previously (Kreyling et al. 2002). A titanium electrode was used and the spark was generated in an oxygen stream. The stoichiometry ratio of synthesized amorphous TiO_2 was confirmed using electron energy loss spectrometry (EELS). Rutile TiO_2 nanoparticles were prepared by annealing anatase TiO_2 nanoparticles in the furnace reactor. Two commercially available TiO_2 samples, Degussa P25 and Fisher anatase TiO_2, were also tested in this study.

The synthesized TiO_2 nanoparticles were well characterized using different analytical techniques. During the synthesis process, the particle mobility size distributions were measured online using a scanning mobility particle spectrometry (SMPS) including a differential mobility analyzer (DMA, Model 3081, TSI Inc.) and a condensation particle counter (CPC 3022, TSI Inc.). After particle collection on the filter paper, scanning electron microscopy (SEM, S-4500, Hitachi) and transmission electron microscopy (TEM, 1200, JEOL) were used to characterize their morphology and measure the primary particle size distribution. X-ray diffraction (XRD) patterns of collected samples were measured using a Rigaku Geigerflex D-MAX/A Diffractometer with Cu-Kα radiation. Based on the diffraction patterns, the weight fractions of each phase for mixed anatase and rutile samples were calculated (Spurr and Myers 1957). The crystallite sizes of crystalline TiO_2 nanoparticles were estimated using the Scherrer equation. BET isotherms (Autosorb-1, Qantachrome) were used to measure the specific surface area of the nanoparticles with nitrogen adsorption at 77K. The BET equivalent particle diameter was calculated based upon the specific surface area and the particle density.

2.2 Nanoparticle Oxidant Generating Capacity Measurements

ROS refers to a class of compounds with strong oxidizing ability and they have been implicated in causing several adverse biological effects (Venkatachari et al. 2005; Xia et al. 2006). The ability of nanoparticles to generate ROS was measured by using a fluorescent dye, 2′,7′-

NIH-PA Author Manuscript

NIH-PA Author Manuscript

NIH-PA Author Manuscript

dichlorofluorescein diacetate (DCFH-DA). Sodium hydroxide was used to cleave the acetate group from the reduced dye (DCFH). In the presence of hydrogen peroxide (H_2O_2) or oxidizing species generated by nanoparticles, DCFH was oxidatively modified into a highly fluorescent derivative, dichlorofluorescein (DCF), which was detected using a spectrofluorometer (absorbance/emission maxima, 485 nm/535 nm). Horseradish peroxidase (HRP) was added to enhance the oxidation of DCFH. Experiments using particles with high reactivity (nanosized Ag) showed that the removal of HRP from the system reduced the ROS activity to background level. Particle suspensions in sodium phosphate buffer with DCFH and HRP were incubated in a 37°C water bath for 15 minutes (in the dark) before measuring the fluorescence intensity of the sample. For comparison, blanks (without nanoparticles) and the standard solutions with known H_2O_2 concentration were also incubated and measured. By comparing the DCF produced in particle suspensions to the DCF produced in H_2O_2 standard solutions, the level of ROS generated by nanoparticles was determined and expressed as equivalent H_2O_2 concentration. Two different suspension particle mass concentrations, 50 μg/ml and 100 μg/ml, were used for each TiO_2 sample. As these are chemical tests, and the samples are very well controlled, error estimates in the ROS data are not illustrated from the duplicate measurements.

3. Results

3.1 Nanoparticle Characterization

All the samples with selected properties are summarized in Table 1, including the crystal phase information, the BET specific surface area and the BET equivalent particle diameter as calculated from the specific surface area, the primary particle diameter measured by TEM/SEM and the crystallite size. As prepared, TiO_2 samples can be categorized into particles of different sizes and same crystal phases and particles of similar sizes and different crystal phases. For all TiO_2 samples (3 - 195 nm), the primary particle size agreed very well with the BET equivalent diameter. The size characterization of two anatase TiO_2 samples (No. 1 and 7) is discussed here as an example. Both the primary particle size distribution measured by TEM/SEM and the mobility based size distribution measured by SMPS were log-normal in shape (Figure 1). The geometric mean diameters of both the primary particle size distribution and the mobility based size distribution were in excellent agreement with the corresponding BET equivalent diameters. For both large sized TiO_2 sample (No. 7) and small sized TiO_2 sample (No. 1), the mobility based particle size distribution agreed very well with the primary particle size distribution, which implies that most particles were unagglomerated and spherical (Jiang et al. 2007). The spherical shape was clearly visible in the TEM/SEM images. The crystallinity of synthesized TiO_2 samples was also well characterized. TiO_2 nanoparticles with different crystal structures were prepared, which included amorphous structure, anatase, rutile and anatase/rutile mixture of different ratios. The XRD patterns of four different representatives (No. 6, 15, 19 & 21) are shown in Figure 2.

3.2 Size Effect

The effect of nanoparticle size on ROS generation was studied by using anatase TiO_2 nanoparticles of 9 different sizes. The choice of the appropriate dose metric was also examined. In traditional toxicology studies, mass is used as the metric and often used to represent the exposure concentration. The measured ROS (expressed as equivalent H_2O_2 concentration) in particle suspensions for two mass concentrations of nanomaterials (50 μg/ml and 100 μg/ml) was plotted as a function of size in Figure 3a. For same sized particles, ROS generation was nearly doubled when doubling the TiO_2 mass concentration (Figure 3a). 30 nm particles showed the highest activity in terms of ROS species generation at both mass concentrations. This seems to be consistent with the photoactivity results of TiO_2 nanoparticles, where the optimum effective size for TiO_2 photoactivity has been reported to be in the range of 25 - 40 nm (Almquist and Biswas 2002). However, no size effect is discernable, as the total surface

NIH-PA Author Manuscript

NIH-PA Author Manuscript

NIH-PA Author Manuscript

area is not held constant for all the samples (higher for the smaller sized particles at the same mass concentration).

It has been proposed that a simple term such as the total surface area or particle number can be used to describe the dose-response curve (Kuempel et al. 2006; Oberdorster et al. 2005b; Wittmaack 2007). Therefore, the results of the equivalent H_2O_2 concentration (measure of ROS) was plotted as a function of the total number concentration (Figure 3b) and total surface area concentration (Figure 3c) for different sized anatase TiO_2 samples. The dose-response curve did not exhibit any trend over the full range of particle sizes in the number concentration plot (or the surface area plot).

Plotting the ROS data as a function of particle size does not reveal any trends, therefore the ROS data was normalized by expressing the equivalent ROS activity per unit of the different dose metrics of mass, number, and surface area (Figure 4). As shown in Figure 4a and 4b, the ROS activity per unit mass or number collapses onto a single curve; but the size dependency is still not clear. However, when normalized by the total surface area, a clear relationship is observed in the form of an S-shaped curve (Figure 4c). Three size ranges can be established: below 10 nm, above 30 nm, and from 10 nm to 30 nm. In the first two ranges, the ROS activities per unit area of TiO_2 particles were relatively constant, while a sharp increase was observed in the third range. A detailed interpretation of this trend is described in the Discussion section.

3.3 Crystal Phase Effect

The effect of crystal phase on TiO_2 activity was evaluated by measuring the oxidant capacity of TiO_2 nanoparticles with similar sizes. The investigated crystal phases included amorphous, anatase, rutile and anatase/rutile mixtures of different ratios. As illustrated in the previous section about the effect of size on TiO_2 activity, the ROS activities per unit area of TiO_2 particles smaller than 10 nm and larger than 30 nm are not a strong function of particle size. Therefore, these two size ranges can be used to study the crystal structure effect on TiO_2 activity without worrying about the interference from a size effect. In the small size range (<10 nm), 3 nm amorphous TiO_2 nanoparticles were compared to 4 nm anatase TiO_2 nanoparticles. As shown in Figure 5a, amorphous TiO_2 particles have much higher ROS activity than anatase TiO_2 under a given mass loading (50 μg/ml). Since their size and specific surface area were close to each other, the normalization by surface area concentration did not change the trend that in this size range amorphous TiO_2 nanoparticles were more active than anatase TiO_2 nanoparticles in terms of ROS generation (Figure 5b).

A more complete evaluation of the effect of crystal structure on TiO_2 toxic potential was performed by comparing the oxidant capacity of thirteen larger-sized TiO_2 samples (> 30 nm) with different crystal structures. As shown in Figure 5a, in the large size range, amorphous TiO_2 particles produced more ROS than anatase TiO_2 particles with the same sizes, which is consistent with the observation in the small size range (< 10 nm). It was also clear that 100% anatase TiO_2 particles had higher ROS activities than anatase/rutile mixtures with the same sizes (40 nm and 50 nm). As the rutile fraction increased, however, a clear relationship could not be established prior to normalization by the surface area concentration, since surface area effect of different sized TiO_2 particles exists under a given mass concentration. After normalization, it became apparent that rutile TiO_2 particles had lower ROS activity than both amorphous and anatase TiO_2 (Figure 5b), as did anatase/rutile mixtures. Although three samples (61%, 55% and 40% anatase) slightly deviated from this relationship, the general trend appeared to be that the ROS activity of anatase/rutile TiO_2 decreased as the fraction of rutile increased.

NIH-PA Author Manuscript

NIH-PA Author Manuscript

NIH-PA Author Manuscript

4. Discussion

Similar to the photocatalytic activity of TiO_2 that is not directly proportional to the total surface area but to the availability of active sites (Sclafani and Herrmann 1996), the same is true for ROS activity of TiO_2. The discontinuous crystal planes or defects in the crystal structures of nanomaterials play an important role in reactive oxygen species generation; and hence nanoparticle activity is related to the available surface defect sites (Arenz et al. 2005; Rajh et al. 2002). A greater number of defects per unit surface area translates into greater activity. Small TiO_2 particles (less than 30 nm in this work) have a lower number of defect sites per unit surface area compared to larger particles of the same crystal phase (Banfield and Zhang 2001). This explains the decrease observed in Figure 4c below 30 nm. These results are consistent with observations from TiO_2 surface absorption activity tests. For example, after normalization by total surface area, small sized TiO_2 nanoparticles have lower adsorption affinity and capacity for lead (Pb) than larger sized particles (Giammar et al. 2007). Similarly, the adsorption of Cd(II) on anatase TiO_2 occurred with lower affinities for smaller sized nanoparticles than for larger particles (Gao et al. 2004). Other materials have also exhibited a size dependent surface defect density. A decrease in surface area normalized adsorption density with decreasing particle size was observed for adsorption of Hg(II) on nanoscale goethite (α-FeOOH) (Waychunas et al. 2005).

For particles greater than 30 nm in size, the ROS activity per unit surface area was similar for different sized particles (30 - 195 nm, Figure 4c) as they behave similarly to bulk anatase TiO_2 (number of reactive or defect sites per unit surface area is constant). Below 10 nm, the ROS generation per unit surface area is also approximately the same (Figure 4c) due to the number of reactive sites being constant per unit surface area. One reason for this could be that particles below 10 nm are synthesized by quenching the particle growth by very rapid dilution (Almquist and Biswas 2002; Jiang et al. 2007). Due to this, the number of reactive sites per unit area may not decrease further with decrease in size but remain approximately constant. The overall low reactivity of particles in the quantum regime can also be attributed to decrease in electron populations at the higher energy bands of titanium dioxide, due to increased separation of energy states.

Using the understanding that was developed by plotting the results with the ROS normalized by surface area allows a clearer interpretation of the trends with size. This reasoning can then be used to explain the trends in Figure 3, which is a more commonly adopted way of presenting results in the toxicology literature. Above 30 nm, the reactivity of anatase TiO_2 nanoparticles is directly proportional to the total surface area (Figure 3c). Similarly, the trends in Figure 3a can also be explained readily. In the range of 30 -195 nm and below 10 nm, the ROS activity is proportional to the surface area. Therefore, the intrinsic ROS activity of particles in the 30-200 nm size range increases with decreasing particle size for a given mass loading, and this non-biological activity is similar to what was reported in previous toxicological studies (Donaldson et al. 2001a;Oberdorster et al. 2005b). The same reasoning holds for anatase TiO_2 particles in the size range of 4 - 10 nm, i.e. they had similar ROS activity and smaller particles generated more ROS at a fixed mass loading (due to their larger total surface area).

In summary, the reactivity depends on the defect site density (number of defects per unit area). The defect site density is approximately constant above 30 nm, decreases between 30 and 10 nm, and then is very low and approximately constant for particles below 10 nm. This variation is a strong function of the synthesis method (Mills and LeHunte 1997), and caution should be exercised in comparing activity of samples prepared by different methodologies and systems. Clear trends could be deciphered in this work due to the large number of available samples that were produced with very strict control of properties. It would also be important to

NIH-PA Author Manuscript

NIH-PA Author Manuscript

NIH-PA Author Manuscript

determine whether such an S-shaped dose-response curve would be observed in biological *in vitro* and *in vivo* tests.

The trend in size is consistent for TiO_2 particles with other crystal structures (anatase/rutile mixture and amorphous). The oxidant capacity of 60 nm (No. 10) and 27 nm (No. 11) TiO_2 nanoparticles, which were 80% anatase and 20% rutile, was measured. Similar to anatase TiO_2, smaller anatase/rutile TiO_2 particles had lower ROS activity per unit surface area than larger ones (1.19 μmol/m^2 vs. 2.43 μmol/m^2). For a given mass loading, however, the total surface area increase for 27 nm particles was large enough to overcome the activity decrease so that slightly more reactive oxygen species were produced by 27 nm particles (3.41 μM vs. 3.10 μM). For amorphous TiO_2 with different sizes, the trend was similar (Figure 5). 53 nm amorphous particles (No. 22) had a similar ROS activity per unit area as 41 nm amorphous particles (No. 21), and this was much higher than 3 nm amorphous particles (No. 20), as shown in Figure 5b. However, 3 nm particles had a much higher total surface area and subsequently generated more reactive oxygen species under the same mass loading of 50 μg/ml (35.3 μM vs 7.5 μM or 6.2 μM; Figure 5a).

The phase composition effect on TiO_2 ROS activity also derives from particle structure characteristics, especially surface properties. Amorphous TiO_2 has much higher surface defect density compared to anatase and rutile TiO_2 since its structure is not periodic (Carp et al. 2004). These defects serve as active sites and generate ROS. Therefore, in the similar size range, amorphous TiO_2 particles have a higher intrinsic oxidant capacity compared to crystalline TiO_2 particles. The observation that anatase TiO_2 has higher ROS activity than rutile TiO_2 is consistent with the results of other activity tests. It has been reported that anatase is more photocatalytically active than rutile (Carp et al. 2004; Sclafani and Herrmann 1996). The lead (Pb) absorption affinity and capacities of anatase were demonstrated to be higher than that of rutile (Giammar et al. 2007). Samples of the mixed phase materials fell in between these two extremes in ROS activity, catalytic activity and adsorption activity. Similar results were also reported by Sayes and coworkers (Sayes et al. 2006) in cytotoxicity tests using TiO_2 nanoparticles with different crystal structures, although the sizes of their TiO_2 samples were not the same. The higher activity of anatase with respect to that of rutile could be explained by their surface chemistry difference, i.e. the higher aptitude of anatase to adsorb oxygen in the form of O_2^- and O^- (Sclafani and Herrmann 1996) and the dissociative adsorption of water molecules to anatase faces (i.e. as H^+ and OH^-) against the nondissociative water adsorption to rutile faces (i.e. as H_2O) (Selloni et al. 1998; Vittadini et al. 1998). Oxygen in the form of O_2^-, O^- and dissociated water molecules on the anatase crystal faces facilitate the ROS formation (Sclafani and Herrmann 1996).

Though only chemical activity was measured in this study, this is very relevant to toxicological studies. The intrinsic non-biological oxidant capacity could be used as a pre-screening strategy to predict nanoparticle toxic potential. However, the validity of this suggestion needs to be determined in subsequent toxicity tests using a range of particle sizes (<10 nm to >30 nm) with well defined crystal structure in cell and animal studies, which is the subject of future studies in our group. Importantly, nanoparticle-cell interactions – *in vitro* or *in vivo* – will also result in cell activation, with additional ROS production by different cellular mechanisms (Donaldson et al. 2006; Nel et al. 2006; Oberdorster et al. 2007) that are likely to be dependent upon particle surface properties and intracellular targets. The method of presenting the data proposed in this paper allows an evaluation of the true effects of parameters such as size. For example, to study the effect of size, it is suggested that the biological signal (such as inflammation, gene and protein expression, oxidative stress, or other) is presented per unit surface area for the different sizes. Additional ROS production by cells mentioned above as well as possibly differences between BET surface area and bio-available surface area have to be considered when interpreting *in vitro* and *in vivo* results. Thus, agglomeration of particles could be one important

NIH-PA Author Manuscript

NIH-PA Author Manuscript

NIH-PA Author Manuscript

factor. All the particles used in this study tended to agglomerate to different degrees in solution (the hydrodynamic sizes of 10 nm and 50 nm particles in deionized water were 140 nm and 525 nm, respectively). While not important in establishing chemical activity relationships as the surface of the particle is still available, it may be an important factor that would influence the results of the *in vivo* or *in vitro* studies.

5. Conclusions

Due to the availability of a large number of well controlled samples of TiO_2 nanoparticles that were synthesized by aerosol routes, a detailed evaluation of ROS activity as a function of physico-chemical properties could be carried out. Keeping the synthesis method the same allowed better control of the defect sites which were an indicator of chemical activity. To establish the true effect of particle size, different metrics were examined – and it was established that the ROS generation per surface area allowed for developing a clear understanding of the trends. An S-shaped curve for ROS activity per surface area as a function of particle size was obtained for the same crystal phase of titanium dioxide nanoparticles. For particles larger than 30 nm, the activity per unit area was constant, followed by a decrease when particle size decreased from 30 nm to 10 nm, and constant values for particles smaller than 10 nm. It is expected that all nanoparticles would exhibit a similar behavior, however, the dependence is a strong function of the exact synthesis procedures used. Such S-shaped curves may also be used to more precisely define particle sizes of importance; for example, greater than 30 nm being defined as bulk sizes, between 30 and 10 nm as the nanometer size regime, and less than 10 nm as the quantum regime (rather than an arbitrary definition for all nanoparticles to be less than 100 nm). The oxidant reactivity exhibited by TiO_2 particles with similar size but different crystal structures was highest for amorphous samples, followed by pure anatase, and lower for anatase/rutile mixtures, and lowest for pure rutile.

Acknowledgments

This work was partially supported by a grant from the U.S. Department of Defense (AFOSR) MURI Grant, FA9550-04-1-0430. Support from the Center of Materials Innovation, Washington University in St. Louis, and an NIEHS Center Grant (P30 ES01247), University of Rochester are also acknowledged.

References

Almquist CB, Biswas P. Role of synthesis method and particle size of nanostructured TiO2 on its photoactivity. J Catal 2002;212:145–156.

Arenz M, Mayrhofer KJJ, Stamenkovic V, Blizanac BB, Tomoyuki T, Ross PN, et al. The effect of the particle size on the kinetics of CO electrooxidation on high surface area Pt catalysts. J Am Chem Soc 2005;127:6819–6829. [PubMed: 15869305]

Banfield, JF.; Zhang, H. Nanoparticles in the Environment. In: Banfield, JF.; Navrotsky, A., editors. Nanoparticles and the Environment. Vol. 44. Washington, D.C.: The Mineralogical Society of America; 2001.

Biswas P, Wu CY. Critical Review: Nanoparticles and the environment. J Air Waste Manage 2005;55:708–746.

Carp O, Huisman CL, Reller A. Photoinduced reactivity of titanium dioxide. Prog Solid State Ch 2004;32:33–177.

Donaldson K, Aitken R, Tran L, Stone V, Duffin R, Forrest G, et al. Carbon nanotubes: A review of their properties in relation to pulmonary toxicology and workplace safety. Toxicol Sci 2006;92:5–22. [PubMed: 16484287]

Donaldson K, Brown D, Clouter A, Duffin R, MacNee W, Renwick L, et al. The pulmonary toxicology of ultrafine particles. J Aerosol Med 2002;15:213–220. [PubMed: 12184871]

Donaldson K, Stone V, Clouter A, Renwick L, MacNee W. Ultrafine particles. Occup Environ Med 2001a;58:211–216. [PubMed: 11171936]

NIH-PA Author Manuscript

NIH-PA Author Manuscript

NIH-PA Author Manuscript

Donaldson K, Stone V, Seaton A, MacNee W. Ambient particle inhalation and the cardiovascular system: Potential mechanisms. Environmental Health Perspectives 2001;109:523–527. [PubMed: 11544157]

Donaldson K, Tran CL. Inflammation caused by particles and fibers. Inhal Toxicol 2002;14:5–27. [PubMed: 12122558]

Gao Y, Wahi R, Kan AT, Falkner JC, Colvin VL, Tomson AB. Adsorption of cadmium on anatase nanoparticles-effect of crystal size and pH. Langmuir 2004;20:9585–9593. [PubMed: 15491190]

Giammar DE, Maus CJ, Xie LY. Effects of particle size and crystalline phase on lead adsorption to titanium dioxide nanoparticles. Environ Eng Sci 2007;24:85–95.

Harman TC, Taylor PJ, Walsh MP, LaForge BE. Quantum dot superlattice thermoelectric materials and devices. Science 2002;297:2229–2232. [PubMed: 12351781]

Hoshino A, Fujioka K, Oku T, Suga M, Sasaki YF, Ohta T, et al. Physicochemical properties and cellular toxicity of nanocrystal quantum dots depend on their surface modification. Nano Lett 2004;4:2163–2169.

Jiang J, Chen DR, Biswas P. Synthesis of nanoparticles in a flame aerosol reactor (FLAR) with independent and strict control of their size, crystal phase and morphology. Nanotechnology 2007;18:285603.

Kreyling WG, Semmler M, Erbe F, Mayer P, Takenaka S, Schulz H, et al. Translocation of ultrafine insoluble iridium particles from lung epithelium to extrapulmonary organs is size dependent but very low. J Toxicol Env Heal A 2002;65:1513–1530.

Kuempel ED, Tran CL, Castranova V, Bailer AJ. Lung dosimetry and risk assessment of nanoparticles: Evaluating and extending current models in rats and humans. Inhal Toxicol 2006;18:717–724. [PubMed: 16774860]

Magrez A, Kasas S, Salicio V, Pasquier N, Seo JW, Celio M, et al. Cellular toxicity of carbon-based nanomaterials. Nano Lett 2006;6:1121–1125. [PubMed: 16771565]

Maynard AD. Nanotechnology: The next big thing, or much ado about nothing? Ann Occup Hyg 2007;51:1–12. [PubMed: 17041243]

McDonald SA, Konstantatos G, Zhang SG, Cyr PW, Klem EJD, Levina L, et al. Solution-processed PbS quantum dot infrared photodetectors and photovoltaics. Nat Mater 2005;4:138–U14. [PubMed: 15640806]

Mills A, LeHunte S. An overview of semiconductor photocatalysis. J Photoch Photobio A 1997;108:1–35.

Namiki N, Cho K, Fraundorf P, Biswas P. Tubular reactor synthesis of doped nanostructured titanium dioxide and its enhanced activation by coronas and soft X-rays. Ind Eng Chem Res 2005;44:5213–5220.

Nel A, Xia T, Madler L, Li N. Toxic potential of materials at the nanolevel. Science 2006;311:622–627. [PubMed: 16456071]

Oberdorster E. Manufactured nanomaterials (Fullerenes, C-60) induce oxidative stress in the brain of juvenile largemouth bass. Environ Health Persp 2004;112:1058–1062.

Oberdorster G. Toxicology of ultrafine particles: in vivo studies. Phil Trans R Soc Lond A 2000;358:2719–2740.

Oberdorster G, Maynard A, Donaldson K, Castranova V, Fitzpatrick J, Ausman K, et al. Principles for characterizing the potential human health effects from exposure to nanomaterials: elements of a screening strategy. Particle and Fibre Toxicology 2005a;2:8. [PubMed: 16209704]

Oberdorster G, Oberdorster E, Oberdorster J. Nanotoxicology: An emerging discipline evolving from studies of ultrafine particles. Environ Health Persp 2005b;113:823–839.

Oberdorster G, Stone V, Donaldson K. Toxicology of nanoparticles: A historical perspective. Nanotoxicology 2007;1:2–25.

Okuyama K, Kousaka Y, Tohge N, Yamamoto S, Wu JJ, Flagan RC, et al. Production of ultrafine metal oxide aerosol particles by thermal decomposition of metal alkoxide vapors. AICHE J 1986;32:2010–2019.

Penttinen P, Timonen KL, Tiittanen P, Mirme A, Ruuskanen J, Pekkanen J. Ultrafine particles in urban air and respiratory health among adult asthmatics. Eur Respir J 2001;17:428–435. [PubMed: 11405521]

NIH-PA Author Manuscript

NIH-PA Author Manuscript

NIH-PA Author Manuscript

Rajh T, Chen LX, Lukas K, Liu T, Thurnauer MC, Tiede DM. Surface restructuring of nanoparticles: An efficient route for ligand-metal oxide crosstalk. J Phys Chem B 2002;106:10543–10552.

Roco MC. Nanoscale science and engineering: Unifying and transforming tools. AICHE J 2004;50:890–897.

Rosner DE. Flame synthesis of valuable nanoparticles: Recent progress/current needs in areas of rate laws, population dynamics, and characterization. Ind Eng Chem Res 2005;44:6045–6055.

Sayes CM, Wahi R, Kurian PA, Liu YP, West JL, Ausman KD, et al. Correlating nanoscale titania structure with toxicity: A cytotoxicity and inflammatory response study with human dermal fibroblasts and human lung epithelial cells. Toxicol Sci 2006;92:174–185. [PubMed: 16613837]

Sclafani A, Herrmann JM. Comparison of the photoelectronic and photocatalytic activities of various anatase and rutile forms of titania in pure liquid organic phases and in aqueous solutions. J Phys Chem 1996;100:13655–13661.

Selloni A, Vittadini A, Gratzel M. The adsorption of small molecules on the TiO2 anatase(101) surface by first-principles molecular dynamics. Surf Sci 1998;404:219–222.

Spurr RA, Myers H. Quantitative Analysis of Anatase-Rutile Mixtures with an X-Ray Diffractometer. Anal Chem 1957;29:760–762.

Thimsen E, Biswas P. AICHE J 2007;53:1727–1735.

Venkatachari P, Hopke PK, Grover BD, Eatough DJ. Measurement of particle-bound reactive oxygen species in Rubidoux aerosols. J Atmos Chem 2005;50:49–58.

Vittadini A, Selloni A, Rotzinger FP, Gratzel M. Structure and energetics of water adsorbed at TiO2 anatase (101) and (001) surfaces. Phys Rev Lett 1998;81:2954–2957.

Warheit DB, Webb TR, Reed KL, Frerichs S, Sayes CM. Pulmonary toxicity study in rats with three forms of ultrafine-TiO2 particles: Differential responses related to surface properties. Toxicology 2007;230:90–104. [PubMed: 17196727]

Warheit DB, Webb TR, Sayes CM, Colvin VL, Reed KL. Pulmonary instillation studies with nanoscale TiO2 rods and dots in rats: Toxicity is not dependent upon particle size and surface area. Toxicol Sci 2006;91:227–236. [PubMed: 16495353]

Waychunas GA, Kim CS, Banfield JF. Nanoparticulate iron oxide minerals in soils and sediments: unique properties and contaminant scavenging mechanisms. J Nanopart Res 2005;7:409–433.

Wegner K, Pratsinis SE. Nozzle-quenching process for controlled flame synthesis of titania nanoparticles. AICHE J 2003;49:1667–1675.

Wichmann HE, Peters A. Epidemiological evidence of the effects of ultrafine particle exposure. Phil Trans R Soc Lond A 2000;358:2751–2768.

Wiesner MR, Lowry GV, Alvarez P, Dionysiou D, Biswas P. Assessing the risks of manufactured nanomaterials. Environ Sci Technol 2006;40:4336–4345. [PubMed: 16903268]

Wittmaack K. Search of the most relevant parameter for quantifying lung inflammatory response to nanoparticle exposure: Particle number, surface area, or what? Environ Health Persp 2007;115:187–194.

Xia T, Kovochich M, Brant J, Hotze M, Sempf J, Oberley T, et al. Comparison of the abilities of ambient and manufactured nanoparticles to induce cellular toxicity according to an oxidative stress paradigm. Nano Lett 2006;6:1794–1807. [PubMed: 16895376]

Yang GX, Zhuang HR, Biswas P. Characterization and sinterability of nanophase titania particles processed in flame reactors. Nanostruct Mater 1996;7:675–689.

NIH-PA Author Manuscript

NIH-PA Author Manuscript

NIH-PA Author Manuscript

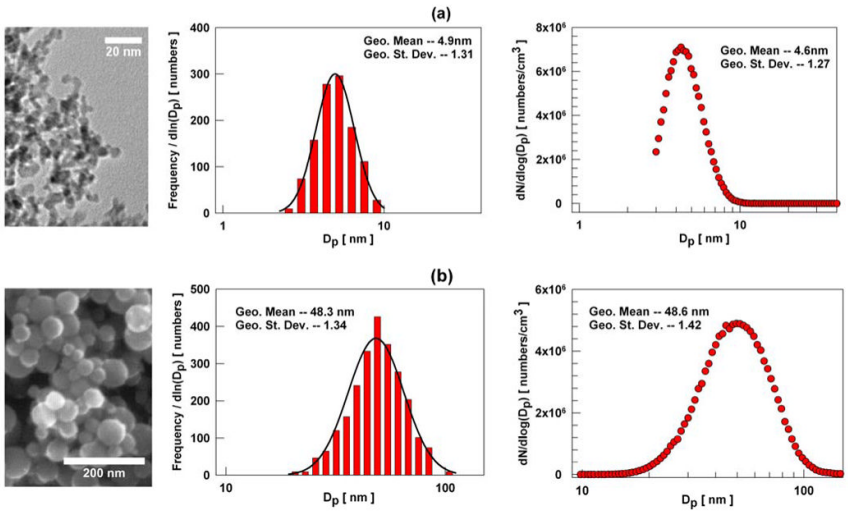

Figure 1.

The primary particle size distributions (middle) measured from electron microscopy images (left) and the mobility based size distributions (right) measured by SMPS of anatase TiO_2 nanoparticles with different sizes: (a) 4 nm (No. 1); (b) 50 nm (No. 7)

NIH-PA Author Manuscript

NIH-PA Author Manuscript

NIH-PA Author Manuscript

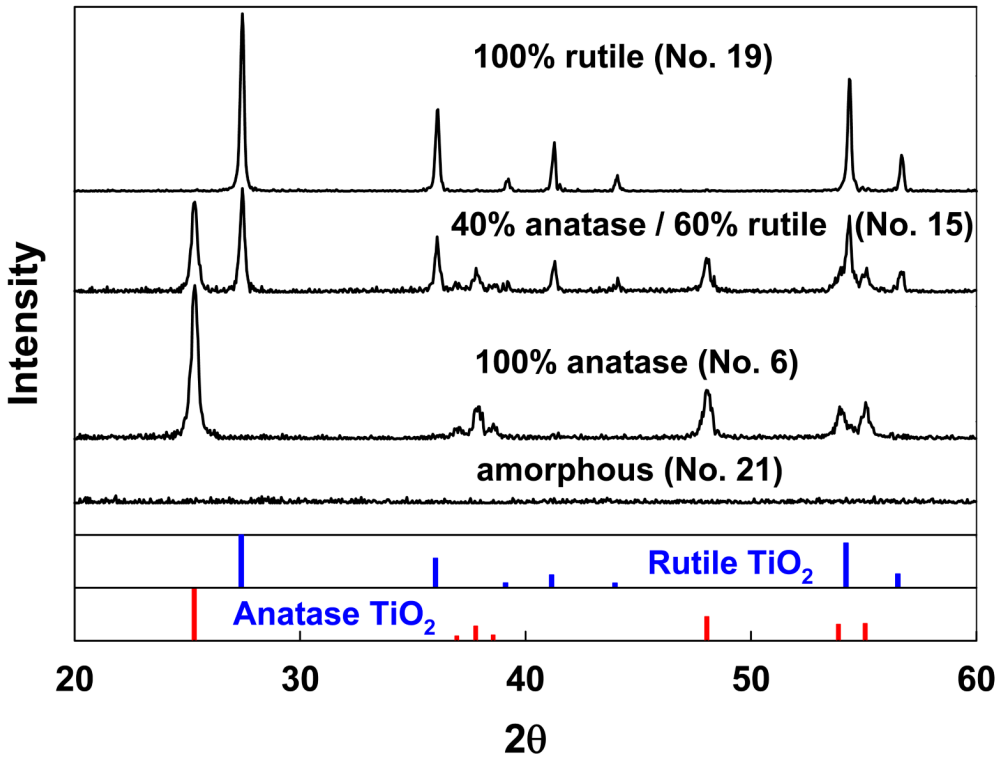

Figure 2.
The XRD spectrums of TiO_2 nanoparticles with different crystal structures

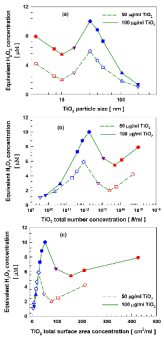

Figure 3.
Reactive oxygen species (ROS) generated by anatase TiO_2 particles of different sizes (No. 1 - 9) versus different dose metrics: (a) particle size; (b) particle number concentration; (c) particle surface area concentration. Different sizes were described by a combination of different symbol and color.

NIH-PA Author Manuscript
NIH-PA Author Manuscript
NIH-PA Author Manuscript

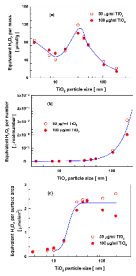

Figure 4.
Reactive oxygen species (ROS) generated by anatase TiO_2 particles of different sizes (No. 1 - 9) normalized by several different dose metrics: (a) particle mass; (b) particle number; (c) particle surface area.

NIH-PA Author Manuscript
NIH-PA Author Manuscript
NIH-PA Author Manuscript

NIH-PA Author Manuscript

NIH-PA Author Manuscript

NIH-PA Author Manuscript

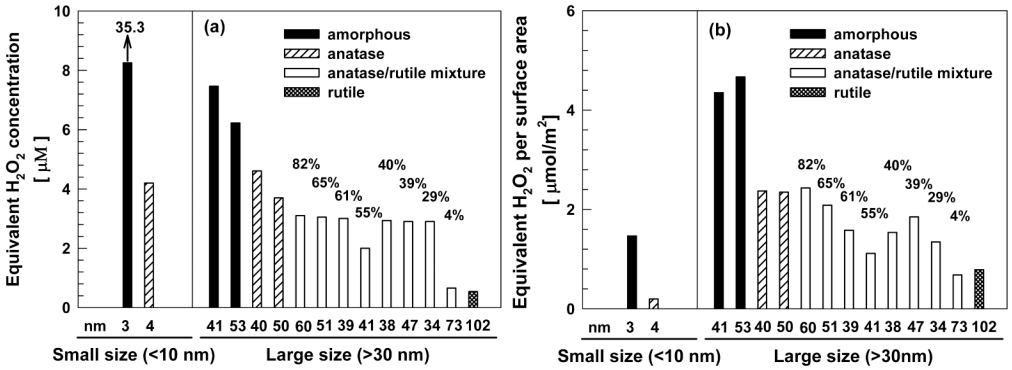

Figure 5.

The reactive oxygen species (ROS) generated by TiO_2 particles of different crystal phases: (a) before, and (b) after normalization by particle surface area concentration.

NIH-PA Author Manuscript NIH-PA Author Manuscript NIH-PA Author Manuscript

Table 1

Summary of Investigated TiO_2 Nanoparticles.

No.	Crystal Phase	S_A[a] (m^2/g)	d_{BET}[b] (nm)	d_p[c] (nm)	d_{XRD}[d] (nm)	Synthesis Method
1	100% anatase	426.1	4	5 ± 1	3.2	*e*
2	100% anatase	209.6	7	8 ± 2	7.7	*e*
3	100% anatase	155.7	10	11 ± 3	10.4	*e*
4	100% anatase	95.80	16	15 ± 4	19.7	*e*
5	100% anatase	51.93	30	30 ± 9	29.1	*f*
6	100% anatase	38.86	40	40 ± 12	30.3	*f*
7	100% anatase	31.52	50	48 ± 14	41.2	*f*
8	100% anatase	14.99	104	98 ± 29	42.0	*f*
9	100% anatase	8.033	195	182 ± 29	67.1	*g*
10	82% anatase/ 18% rutile	25.48	60	56 ± 17	40.9	*f*
11	80% anatase/ 20% rutile	57.44	27	26 ± 8	23.1	*h*
12	65% anatase/ 35% rutile	29.27	51	53 ± 16	41.0	*f*
13	61% anatase/ 39% rutile	38.08	39	38 ± 11	31.8	*f*
14	55% anatase/ 45% rutile	35.95	41	40 ± 12	32.9	*f*
15	40% anatase/ 60% rutile	38.23	38	40 ± 12	31.3	*f*
16	39% anatase/ 69% rutile	31.37	47	45 ± 13	32.7	*f*
17	29% anatase/ 71% rutile	43.12	34	35 ± 10	26.9	*f*
18	4% anatase/ 96% rutile	19.43	73	-	32.1	*i*
19	100% rutile	13.78	102	-	-	*i*
20	amorphous	482.3	3	-	-	*j*
21	amorphous	34.33	41	45 ± 13	-	*k*
22	amorphous	26.67	53	59 ± 21	-	*k*

[a] Specific surface area of particles as measured by N_2 adsorption (BET).

[b] Equivalent particle diameter as calculated from the specific surface area.

[c] Primary particle size as determined by electron microcopy.

[d] Particle crystallite size (anatase) as determined by X-ray diffraction (XRD).

NIH-PA Author Manuscript

NIH-PA Author Manuscript

NIH-PA Author Manuscript

[e] Premixed flame aerosol reactor.

[f] Diffusion flame aerosol reactor.

[g] Commercial available (Fisher Scientific).

[h] Commercial available (Degussa P25).

[i] Annealed in the furnace reactor.

[j] Spark aerosol generator.

[k] Furnace aerosol reactor.